Chemical Physics Letters 508 (2011) 117–120

Contents lists available at ScienceDirect

Chemical Physics Letters

journal homepage: www.elsevier.com/locate/cplett

Synthesis and optical characterization of strong red light emitting $KLaF_4:Eu^{3+}$ nanophosphors

Subrata Das [a], A. Amarnath Reddy [a], Shahzad Ahmad [b], R. Nagarajan [b], G. Vijaya Prakash [a,*]

[a] Nanophotonics Laboratory, Department of Physics, Indian Institute of Technology Delhi, New Delhi 110016, India
[b] Materials Chemistry Group, Department of Chemistry, University of Delhi, New Delhi 110007, India

ARTICLE INFO

Article history:
Received 20 February 2011
In final form 6 April 2011
Available online 9 April 2011

ABSTRACT

Monophasic $KLaF_4$ possessing cubic symmetry with varied Eu^{3+} concentrations were synthesized by wet-chemical reaction. The obtained nanophosphor exhibits nanocrystals of 5 nm size and the dopant Eu^{3+} ions were successfully incorporated into the sites of La^{3+} ions of the host lattice. The dominant red color emission at 612 nm from the hypersensitive ($^5D_0 \rightarrow {}^7F_2$) transition of Eu^{3+} indicates the inversion anti-symmetry crystal field around Eu^{3+} ion, which is favorable to improve the red color purity. Furthermore, the emission life times are high enough and our results broadly suggest the potential application for white LEDs, mercury-free lamps and display panels.

1. Introduction

In recent years, a great deal of research effort has been devoted to the synthesis of rare-earth (Re^{3+}) doped nanocrystalline phosphors due to their novel capabilities resulted from the quantum confinement effects and a high surface-to-volume ratio compared to their bulk counterparts [1–5]. Of these, fluoride nanophosphors such as YF_3 [3], $NaYF_4$ [4,6], GdF_3 [7], LiF [8], and LaF_3 [9] are of special interest due to their many interlinked facts that could influence the emissive nature of Re^{3+} ions. The special class of fluorides, Re^{3+} doped $ALnF_4$ (A = Alkali ion, Ln = rare earth ion) phosphors (for ex: Re^{3+}-doped $NaYF_4$) are attractive, since the host provides very low phonon frequencies, optical transparency over a wide wavelength range and site-selective doping capability [4–6]. Therefore, wide range of applications such as in vivo imaging of tissues and cells, solid state light emitting applications, scintillators and Thermally Stimulated Luminescence (TSL) dosimetry, have been intensely been investigated [6–9]. In general, the emission mechanism of rare-earth ion is critically dependent on the relative energy of the *4f* emitting level, site occupation and guest–host interactions. So far in $ALaF_4$ (A = Na, K) doped phosphor systems, $NaLaF_4$ nanocrystallines, has been widely studies but relatively few studies were reported in $KLaF_4$ nanophosphors [5,10]. Unlike the other fluorides, $KLaF_4$ usually exists in two phases: metastable cubic phase (α-$KLaF_4$) and more stable hexagonal phase (β-$KLaF_4$), depending on the synthetic conditions [5].

Trivalent europium (Eu^{3+}) ion is widely recognized as an activator for red emission (around 612 nm), which has been used in most commercial red phosphors. The intra-4f-shell down-conversion transitions ($^5D_0 \rightarrow {}^7F_j$ (j = 1, 2, 3, 4)) of Eu^{3+} ions are strongly dependent on crystal structure of the host and sensitive to the local environment where the rare-earth has been situated [11,12]. Among all, the red color transition ($^5D_0 \rightarrow {}^7F_2$) of Eu^{3+} is the most intense and hypersensitive transition therefore the transition probabilities are strongly influenced by host lattice, specially the covalent nature of host and site symmetry of the occupation [11,12]. In this Letter, we report monophasic red emitting Eu^{3+} doped $KLaF_4$ nanophosphor, which can be effectively excited by UV/blue/green lights and suitable for use in white LEDs.

2. Experimental

A standard one-step procedure discussed elsewhere was followed for the preparation of $KLaF_4$ nanophosphor [5,13]. Stoichiometric amounts of Potassium Fluoride (KF) and Lanthanum (III) Acetylacetonate ($LaC_{15}H_{21}O_6{\cdot}xH_2O$) and appropriate amount of Europium (III) Chloride ($EuCl_3{\cdot}6H_2O$) were individually dissolved in appropriate amounts of anhydrous methanol and added dropwise (ca. 15–20 min) with constant stirring. Later, the suspension was digested for 1 h after which the product was separated by using ordinary filtration and dried at room-temperature. X-ray diffraction (XRD) data for all these samples was collected on PAN analytical XPERT-PRO diffractometer with $CuK\alpha_1$ source (λ = 1.5405 Å). The steady-state and time-resolved emission measurements were carried using home built setups using 532 nm diode laser as excitation source, wherein the emission light was dispersed into a monochromator (Acton SP2300) coupled to a photo multiplier tube (PMT) through appropriate lens system. For time-resolved measurements, mechanical chopper (12 Hz), lock-in amplifier, and digital storage oscilloscope were employed.

* Corresponding author. Fax: +91(0) 11 2658 1114.
E-mail address: prakash@physics.iitd.ac.in (G. Vijaya Prakash).

0009-2614/$ - see front matter © 2011 Elsevier B.V. All rights reserved.
doi:10.1016/j.cplett.2011.04.029

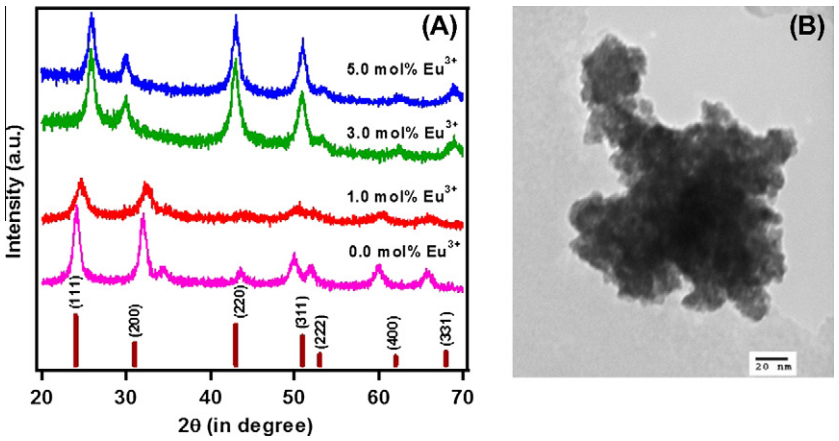

Figure 1. Room temperature (A) X-ray diffraction pattern of x mol% (x = 0, 1, 3, 5) Eu^{3+}-doped $KLaF_4$ nanophosphor. The XRD patterns were indexed according to the JCPDS data No. 75–2020. (B) TEM image of 5 mol% Eu^{3+}-doped $KLaF_4$ nanophosphor.

3. Results and discussions

3.1. XRD and TEM studies

The X-ray diffraction patterns of x mol% (x = 0, 1, 3, 5) Eu^{3+}-doped $KLaF_4$ phosphors are presented in Figure 1A and the all the obtained patterns are identified as cubic $KLaF_4$ having space group *Fm3m* (JCPDS File No. 75-2020) [14]. It is known that $KLaF_4$ exhibit two phases, namely, α-phase (cubic) and β-phase (hexagonal) depending on the synthesis conditions [5]. The α-phase $KLaF_4$ is a metastable high-temperature phase and is isomorphic with that of CaF_2, wherein the K^+ and La^{3+} ions are randomly coordinated and each cation is coordinated by F^- ion again [5]. As seen from Figure 1A, upon Eu^{3+} ion doping, the diffraction peaks are slightly shifted to the higher side by about 1–2° angles. These shifts in the XRD peaks are attributed to the substitution of the larger ionic radius La^{3+} ions (117 pm) by comparatively smaller ionic radius Eu^{3+} ions (108 pm) in host lattice [7,15]. This is further indicating that Eu^{3+} ions have been successfully doped into the crystal lattice of $KLaF_4$ host. In addition, the (2 2 0) and (3 1 1) peaks exhibit significant broadening with enhanced intensity, which may be attributed to the disorder in the (2 2 0) and (3 1 1) sides of $KLaF_4$:Eu^{3+} [16]. The estimated cubic lattice parameter for the x mol% (x = 0, 1, 3, 5) Eu^{3+}-doping were 6.38 (0), 6.26 (1), 5.95 (3), 5.94 (5) Å respectively. The decrease in lattice parameters with the increase of Eu^{3+}-doping is reasonable, since Eu^{3+} ions are selectively replaces the sites of much larger ionic radius sites of La^{3+} ions. The broad diffraction peaks indicating the decrease in crystal size and the average crystallite sizes estimated from the Scherrer analysis were in the range of 5–15 nm. The TEM image (Figure 1B) of 5 mol% Eu^{3+}-doped $KLaF_4$ shows that the sample precipitates into agglomerated nanosized particles of average grain size 5 nm, which is close to the particle size estimated from XRD data.

3.2. Photoluminescence studies

The room temperature PL spectra of x mol% (x = 1, 3, 5, 10) Eu^{3+}-doped $KLaF_4$ nanophosphors under 532 nm laser, is shown in the Figure 2A. The spectra consists of several emission peaks at 579, 594, 612, 650 and 701 nm which are corresponds to Eu^{3+} ion transitions, $^5D_0 \rightarrow {}^7F_J$ (J = 0, 1, 2, 3, 4) respectively. Out of all, the hypersensitive electric dipole transition at 612 nm ($^5D_0 \rightarrow {}^7F_2$ of Eu^{3+}) was found to be intense, which is responsible for the bright orange-red luminescence and the corresponding intensities shows a systematic enhancement with the increase of Eu^{3+}-doping concentration. The red color intensity of the phosphor is even visible to the naked eye (Inset of Figure 2A). The $^5D_0 \rightarrow {}^7F_0$ is basically a forbidden transition due to the same J = 0 value. Another intense line $^5D_0 \rightarrow {}^7F_1$ (orange) is a magnetic dipole transition. The hypersensitive $^5D_0 \rightarrow {}^7F_2$ (at 612 nm) transition is highly sensitive to the site occupation of Eu^{3+} ions of inversion or anti-inversion symmetry. The orange color ($^5D_0 \rightarrow {}^7F_1$) emission dominates when Eu^{3+} ions occupy the sites of inversion symmetry. However, the lower crystal symmetry and subsequently the dominant red color

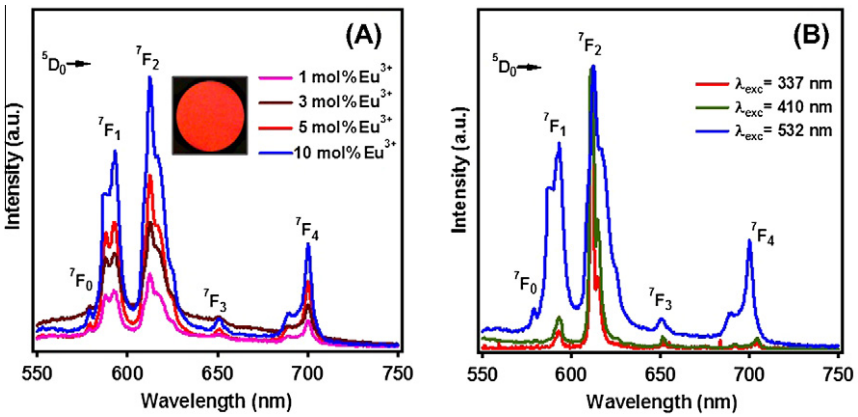

Figure 2. Room temperature emission spectra of (A) x mol% (x = 1, 3, 5, 10) Eu^{3+} doped in $KLaF_4$ nanophosphor (λ_{exe} = 532 nm) and (B) 10 mol% Eu^{3+}-doped $KLaF_4$ nanophosphor with different excitation wavelengths.

Table 1
The emission life times of 612 nm ($^5D_0 \rightarrow {}^7F_2$ of Eu^{3+}) and Red-to-Orange ($^5D_0 \rightarrow {}^7F_2/{}^5D_0 \rightarrow {}^7F_1$ of Eu^{3+}) (R/O) intensity ratios of various Eu^{3+}-doped $KLaF_4$ nanophosphors (λ_{exe} = 532 nm). The R/O ratios and emission life times of several reported Eu^{3+} doped phosphors are also given for comparison.

Phosphor	Life time 'τ' (ms)	R/O ratio	Reference
$KLaF_4$:1 mol%Eu^{3+}	2.86	1.29	Present work
$KLaF_4$:3 mol%Eu^{3+}	4.30	1.33	Present work
$KLaF_4$:5 mol%Eu^{3+}	5.40	1.35	Present work
$KLaF_4$:10 mol%Eu^{3+}	6.90	1.38	Present work
GdF_3:5 mol%Eu^{3+}	4.80	1.31*	[7]
CaF_2:1.5 mol%Eu^{3+}	2.08	1.43*	[22]
$NaYF_4$:10 mol%Eu^{3+}	6.20	1.59*	[23]
$LaVO_4$:20 mol%Eu^{3+}	0.12	1.43*	[24]
$CaSc_2O_4$:6 mol%Eu^{3+}	1.00	1.30*	[25]
$CaSiO_3$:4 mol%Eu^{3+}	3.30	1.65*	[26]
Y_2SiO_5:1 wt%Eu^{3+}	2.10	2.71	[27]
$InVO_4$:30 mol%Eu^{3+}	0.83	2.33*	[28]
YVO_4:2 mol%Eu^{3+}	0.54	1.24*	[29]
YPO_4:2 mol%Eu^{3+}	2.89	1.99*	[29]
La_2O_3: Eu^{3+}	1.38	3.98	[30]

* Estimated R/O values from respective references.

($^5D_0 \rightarrow {}^7F_2$) purity can be achieved by introducing high degree of disorder, either by particle size reduction or introducing metallic and nonmetallic elements, as reported by many authors [30–33]. The dominant red emission from $^5D_0 \rightarrow {}^7F_2$ transition indicates the inversion anti symmetry crystal field around Eu^{3+} ion in the present nanophosphor, which is favorable to improve the color purity of the red phosphor [16,17]. Moreover, the XRD patterns show that Eu^{3+} ions are successfully incorporated into the sites of La^{3+} in $KLaF_4$ lattice, which is further supporting the emission characteristics.

In general, the transition probability of the magnetic-dipole transition $^5D_0 \rightarrow {}^7F_1$ is nearly independent on the host matrix and the electric-dipole allowed $^5D_0 \rightarrow {}^7F_2$ transition is strongly influenced by the local structure and site asymmetry around Eu^{3+} ion [17,18]. Therefore, the emission intensity ratio between red and orange (R/O) color transitions corresponding to $^5D_0 \rightarrow {}^7F_2$ and $^5D_0 \rightarrow {}^7F_1$ is widely known as the asymmetric ratio. The R/O ratios of the present nanophosphors, for different Eu^{3+}-doping concentration, are calculated from the emission spectra (Figure 2A) and the values are listed in Table 1. The relative R/O ratios as a function of the Eu^{3+} content in $KLaF_4$ nanophsohors are nearly same (1.29–1.38), indicating that the overall Eu^{3+} local environments are almost same for different concentrations. Therefore, it can be speculated that the Eu^{3+} ions are conveniently occupied the sites of La^{3+} in the crystal lattice of $KLaF_4$ [16,19].

To further illustrate the emission characteristics and the excitation wavelength dependence, several excitation wavelengths of commercially available excitation sources are used (Figure 2B). The emission results show no spectral shift under different excitations and gives stable color purity at red-end wavelengths, which is favorable for LED applications. However, the excitations less than 532 nm, the R/O ratios are more than 2 and such values are comparable to those reported for oxide phosphors. The R/O ratios of several reported Eu^{3+} doped oxide and fluoride based phosphors are also given for comparison in Table 1. A simple schematic energy level diagram illustrating the excitation and emission transitions of Eu^{3+} ions is shown in Figure 3A.

The emission intensity decay profiles for the 612 nm ($^5D_0 \rightarrow {}^7F_2$ of Eu^{3+}) emission of the $KLaF_4$:Eu^{3+} nanophosphors were recorded and the decay curves fits into a single-exponential function $I = I_0 \exp(-t/\tau)$ (I_0 is the initial emission intensity at $t = 0$) (see Figure 3B). The emission life time values (τ) obtained from single exponential fits are given in Table 1. The reason for mono-exponential nature is due to homogeneous distribution of doping ions inside the host matrix without any cluster formation [20]. The lifetime (τ) values increases from 2.90 to 6.90 ms as the Eu^{3+}-concentrations increases from 1.0 to 10 mol%. The observed life time values for the present nanophosphors are much higher than the other oxide phosphors and close to the fluoride phosphors (Table 1). These life time values are also consistent with the analogous phosphor $NaYF_4$:Eu^{3+} [23]. While the relative intensities of $^5D_0 \rightarrow {}^7F_2$ of Eu^{3+} emission transition are strongly influenced by their hypersensitivity to local environment, the radiative life times are dependent on various factors such as, covenant nature, polarisability, structural defects and lattice arrangement [20,30–32]. Comparatively larger lifetimes in the present nanophosphors can possibly be attributed to more radiative relaxation caused by surface defects, which can eventually act as luminescent centers. When the surface area increases with decrease in particle size, there are more and more defects which may act as luminescent centers in the sample. Broadly, the emission red-color richness and the larger lifetimes are suitable for potential applications in displays and lights, where high life times are required [21].

4. Conclusion

A strong red-emitting nanophosphor, $KLaF_4$:Eu^{3+}, was synthesized from wet-chemical reactions for the first time. These monophasic nanophosphors show strong dominating red color richness and comparatively longer lifetimes when excited by different wavelengths less than 532 nm. The emission characteristics are

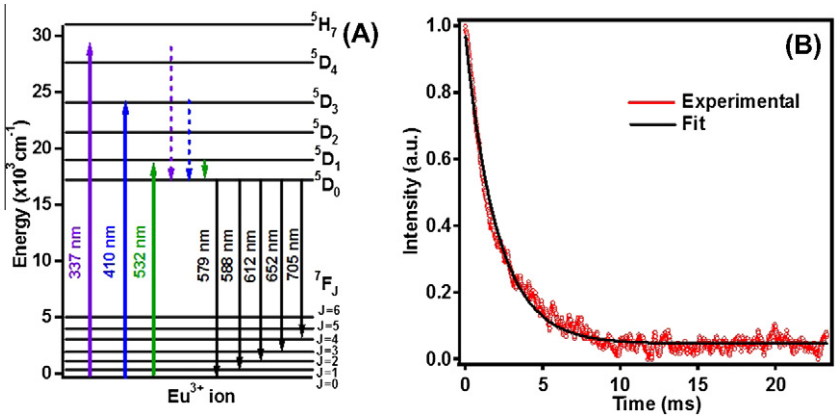

Figure 3. (A) Schematic excitation and emission transition energy level diagram of Eu^{3+} ion. (B) Representative emission decay curve for 612 nm ($^5D_0 \rightarrow {}^7F_2$ of Eu^{3+}) emission of 10 mol% Eu^{3+}-doped $KLaF_4$ nanophosphor (λ_{exe} = 532 nm).

competitive with that of commercial fluoride phosphors such as $GdF_3:Eu^{3+}$ and $CaF_2:Eu^{3+}$. The ability to excite $KLaF_4:Eu^{3+}$ with many commercially available UV, violet and green excitation sources to generate an intense red emission (612 nm) makes these phosphors a very promising material for white light LED and other display applications.

Acknowledgement

Authors acknowledge the financial support from Department of Information Technology (DIT), Govt. of India, under Photonics Development Program (ref: 12(1)/2008-PDD).

References

[1] S. Lu, J. Zhang, J. Zhang, H. Zhao, Y. Luo, X. Ren, Nanotechnology 21 (2010) 365709.
[2] Y. Li, J. Zhang, X. Zhang, Y. Luo, S. Lu, Z. Hao, X. Wang, J. Phys. Chem. C 113 (2009) 17705.
[3] D. Chen, Y. Wang, Y. Yu, P. Huang, Appl. Phys. Lett. 91 (2007) 051920.
[4] G. Wang, Q. Peng, J. Solid State. Chem. 184 (2011) 59.
[5] N. Tyagi, A. Amarnath Reddy, R. Nagarajan, Opt. Mater. 33 (2010) 42.
[6] G.S. Yi, H.C. Lu, S.Y. Zhao, Y. Ge, W.J. Yang, D.P. Chen, L.H. Guo, Nano Lett. 4 (2004) 2191.
[7] X. Zhang, T. Hayakawa, M. Nogami, Y. Ishikawa, J. Alloys Compd. 509 (2011) 2076.
[8] C. Adachi, M.A. Baldo, M.E. Thompson, S.R. Forrest, J. Appl. Phys. 90 (2001) 5048.
[9] S.N. Achary, A.K. Tyagi, T.K. Seshagiri, V.N. Natarajan, Mater. Sci. Eng. B 129 (2006) 256.
[10] Z. Wang, C. Liu, Y. Wang, Z. Li, J. Alloys Compd. 509 (2011) 1964.
[11] Y. Huang, L. Shi, E.S. Kim, H.J. Seo, J. Appl. Phys. 105 (2009) 013512.
[12] Q. Ma, Y. Zhou, A. Zhang, M. Lu, G. Zhou, C. Li, Solid State Sci. 11 (2009) 1124.
[13] G.W. Pope, J.F. Steinbach, W.F. Wagner, J. Inorg. Nucl. Chem. 20 (1961) 304.
[14] W.H. Zachariasen, Acta Crystallogr. 2 (1949) 388.
[15] A. Sarakovskis, J. Grube, A. Mishnev, M. Springis, Opt. Mater. 31 (2009) 1517.
[16] M. Zhong, G. Shan, Y. Li, G. Wang, Y. Liu, Mater. Chem. Phys. 106 (2007) 305.
[17] L. Zhou, J. Wei, J. Wu, F. Gong, L. Yi, J. Huang, J. Alloys Compd. 476 (2009) 390.
[18] B.V. Rao, K. Jang, H.S. Lee, S.S. Yi, J.H. Jeong, J. Alloys Compd. 496 (2010) 251.
[19] G. Vijaya Prakash, R. Jagannathan, Spectrochim. Acta A 55 (1999) 1799.
[20] N.S. Singh, R.S. Ningthoujam, M.N. Luwang, S.D. Singh, R.K. Vatsa, Chem. Phys. Lett. 480 (2009) 237.
[21] C. Qin, Y. Huang, G. Chen, L. Shi, X. Qiao, J. Gan, H.J. Seo, Mater. Lett. 63 (2009) 1162.
[22] L. Song, J. Gao, R. Song, J. Lumin. 130 (2010) 1179.
[23] G. Jia, P.A. Tanner, J. Alloys Compd. 471 (2009) 557.
[24] S.W. Park et al., Phys. B 405 (2010) 4040.
[25] Z. Hao, J. Zhang, X. Zhang, X. Wang, Opt. Mater. 33 (2011) 355.
[26] H. Nagabhushana, B.M. Nagabhushana, M. Madesh Kumar, Chikkahanu mantharayappa, K.V.R. Murthy, C. Shivakumara, R.P.S. Chakradhar, Spectrochim. Acta A 78 (2011) 64.
[27] N. Rakov, D.F. Amaral, R.B. Guimarães, G.S. Maciel, J. Appl. Phys. 108 (2010) 073501.
[28] Y.S. Chang, Z.R. Shi, Y.Y. Tsai, S. Wu, H.L. Chen, Opt. Mater. 33 (2011) 375.
[29] G. Pan et al., J. Appl. Phys. 104 (2008) 084910.
[30] L. Yu, H. Song, Z. Liu, L. Yang, S. Lu, Phys. Chem. Chem. Phys. 8 (2008) 303.
[31] X.C. Jiang, C.H. Yan, L.D. Sun, Z.G. Wei, C.S. Liao, J. Solid State. Chem. 175 (2003) 245.
[32] L. Wang, Y. Wang, J. Mater. Sci. 43 (2008) 2908.
[33] H.Q. Liu, L.L. Wang, S.Q. Chen, B. Zou, J. Lumin. 126 (2007) 459.